Title

Baculovirus AC102 Is a Nucleocapsid Protein That Is Crucial for Nuclear Actin Polymerization and Nucleocapsid Morphogenesis

Journal

Journal of Virology, 92(11)

ISSN

0022-538X

Authors

Hepp, Susan E
Borgo, Gina M
Ticau, Simina
et al.

Publication Date

2018-06-01

DOI

10.1128/jvi.00111-18

Peer reviewed

AMERICAN SOCIETY FOR MICROBIOLOGY | Journal of Virology®

VIRUS-CELL INTERACTIONS

Baculovirus AC102 Is a Nucleocapsid Protein That Is Crucial for Nuclear Actin Polymerization and Nucleocapsid Morphogenesis

Susan E. Hepp,[b] Gina M. Borgo,[c] Simina Ticau,[a]* Taro Ohkawa,[a] Matthew D. Welch[a,b,c]

[a]Department of Molecular and Cell Biology, University of California, Berkeley, California, USA
[b]Graduate Group in Microbiology, University of California, Berkeley, California, USA
[c]Graduate Group in Infectious Diseases and Immunity, University of California, Berkeley, California, USA

ABSTRACT The baculovirus Autographa californica multiple nucleopolyhedrovirus (AcMNPV), the type species of alphabaculoviruses, is an enveloped DNA virus that infects lepidopteran insects and is commonly known as a vector for protein expression and cell transduction. AcMNPV belongs to a diverse group of viral and bacterial pathogens that target the host cell actin cytoskeleton during infection. AcMNPV is unusual, however, in that it absolutely requires actin translocation into the nucleus early in infection and actin polymerization within the nucleus late in infection coincident with viral replication. Of the six viral factors that are sufficient, when coexpressed, to induce the nuclear localization of actin, only AC102 is essential for viral replication and the nuclear accumulation of actin. We therefore sought to better understand the role of AC102 in actin mobilization in the nucleus early and late in infection. Although AC102 was proposed to function early in infection, we found that AC102 is predominantly expressed as a late protein. In addition, we observed that AC102 is required for F-actin assembly in the nucleus during late infection, as well as for proper formation of viral replication structures and nucleocapsid morphogenesis. Finally, we found that AC102 is a nucleocapsid protein and a newly recognized member of a complex consisting of the viral proteins EC27, C42, and the actin polymerization protein P78/83. Taken together, our findings suggest that AC102 is necessary for nucleocapsid morphogenesis and actin assembly during late infection through its role as a component of the P78/83-C42-EC27-AC102 protein complex.

IMPORTANCE The baculovirus Autographa californica multiple nucleopolyhedrovirus (AcMNPV) is an important biotechnological tool for protein expression and cell transduction, and related nucleopolyhedroviruses are also used as environmentally benign insecticides. One impact of our work is to better understand the fundamental mechanisms through which AcMNPV exploits the cellular machinery of the host for replication, which may aid in the development of improved baculovirus-based research and industrial tools. Moreover, AcMNPV's ability to mobilize the host actin cytoskeleton within the cell's nucleus during infection makes it a powerful cell biological tool. It is becoming increasingly clear that actin plays important roles in the cell's nucleus, and yet the regulation and function of nuclear actin is poorly understood. Our work to better understand how AcMNPV relocalizes and polymerizes actin within the nucleus may reveal fundamental mechanisms that govern nuclear actin regulation and function, even in the absence of viral infection.

KEYWORDS actin, baculovirus

Received 21 January 2018 **Accepted** 9 March 2018

Accepted manuscript posted online 14 March 2018

Citation Hepp SE, Borgo GM, Ticau S, Ohkawa T, Welch MD. 2018. Baculovirus AC102 is a nucleocapsid protein that is crucial for nuclear actin polymerization and nucleocapsid morphogenesis. J Virol 92:e00111-18. https://doi.org/10.1128/JVI.00111-18.

Editor Rozanne M. Sandri-Goldin, University of California, Irvine

Address correspondence to Matthew D. Welch, welch@berkeley.edu.

* Present address: Simina Ticau, Ohana Biosciences, Cambridge, Massachusetts, USA.

Autographa californica multiple nucleopolyhedrovirus (AcMNPV), the type species of alphabaculoviruses, is an enveloped DNA virus that infects the larvae of lepidopteran insects (1). Like other NPVs, it has a circular genome (of 134 kb), replicates in the cell's nucleus, and produces two different viral forms, a budded virus (BV) that buds from the plasma membrane and an occlusion-derived virus (ODV) that is enveloped in the nucleus and enclosed in large crystalline bodies called polyhedra. AcMNPV is most commonly used as a vector for protein expression and cell transduction (2). It also belongs to a diverse group of viral and bacterial pathogens that target the host cell actin cytoskeleton during infection by inducing the polymerization of actin monomers (G-actin) into actin filaments (F-actin) to enable intracellular actin-based motility (3, 4). AcMNPV is unusual, however, in that it uses host actin in both the cytoplasm and the nucleus (5, 6) and that it absolutely requires actin polymerization for progeny virus production (7–11).

AcMNPV mobilization of host actin begins immediately after enveloped virions fuse with the plasma membrane or endosomal membrane and viral nucleocapsids are released into the host cell cytoplasm. Nucleocapsids then initiate actin-based motility (12) and form actin comet tails (5, 6), which speeds transit to the nucleus (12). Expression of early viral genes induces the translocation of G-actin into the nucleus, a phenomenon referred to as nuclear localization of actin (NLA) (13). Interestingly, NLA can also be induced in uninfected cells by expressing combinations of six viral genes, including the immediate-early transcriptional transactivator *ie-1*, as well as *pe38*, *ac004*, *ac152*, and either *ac102* or *he65* (13). Of the latter five genes, only *ac102* is essential for viral replication in AcMNPV (14) (as is its ortholog *bm86* in Bombyx mori nucleopolyhedrovirus [15]) and for the nuclear accumulation of G-actin, indicating that it plays a key role in NLA (14).

AcMNPV also mobilizes actin during the late stage of infection (5), when the G-actin that is imported into the nucleus during early infection is polymerized into F-actin in the nuclear ring zone (RZ) (14) surrounding the central virogenic stroma (VS), where DNA replication and nucleocapsid assembly occur. Nuclear F-actin polymerization requires the activity of the viral minor capsid protein P78/83 (encoded by *ac009*), a mimic of host Wiskott-Aldrich Syndrome protein (WASP) family proteins (16) that activates the host Arp2/3 complex to promote actin assembly (9). P78/83 also forms a complex with the viral proteins BV/ODV-C42 (C42; encoded by *ac101*) and ODV-EC27 (EC27; encoded by *ac144*) (17) and associates with one end of the nucleocapsid (18). The genes encoding all three of these proteins are essential for nucleocapsid morphogenesis and the production of BV progeny (9, 19, 20).

To better understand how AcMNPV coordinates actin mobilization early and late in infection, we further investigated the role of NLA factor AC102. We observed that AC102 is predominantly expressed as a late protein. In addition, we observed that AC102 is required for F-actin assembly in the nucleus during late infection, as well as for normal VS formation and nucleocapsid morphogenesis. Finally, we found that AC102 is a nucleocapsid protein and that it copurifies with EC27, C42, and P78/83. Taken together, our findings suggest that AC102 is necessary for nucleocapsid morphogenesis and P78/83-dependent F-actin assembly during late infection through its role as a component of the P78/83-C42-EC27-AC102 protein complex.

RESULTS

AC102 is predominantly expressed late in infection. Although *ac102* was proposed to be expressed as an early gene based on its activity in promoting the NLA phenotype, the *ac102* promoter has both conserved early- and late-sequence features, and *ac102* mRNA is expressed primarily late in infection (21). Nevertheless, the timing of AC102 protein expression had not previously been investigated. We therefore began by determining the temporal expression profile of AC102 by Western blotting using a polyclonal antibody we generated that specifically recognizes AC102 (Fig. 1A). Sf9 cells were infected with AcMNPV strain WOBpos (9), a virus derived from the E2 strain of AcMNPV with a genome that can be replicated and modified as a bacmid in *Escherichia*

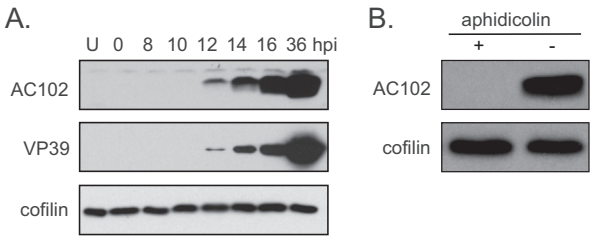

FIG 1 AC102 is predominantly expressed late in infection. (A) Western blots of lysates from uninfected Sf9 cells (U) and cells at various times postinfection with WOBpos at an MOI of 10, probed for AC102, VP39 (a late protein), and cofilin (loading control). (B) Western blots of lysates from WOBpos-infected cells treated with 5 μg/ml aphidicolin (+) or DMSO control (−) at 0 hpi and then processed at 24 hpi and probed for AC102 and cofilin (a loading control).

coli, and AC102 expression was assessed over a range of times postinfection. At 0, 8, and 10 h postinfection (hpi), no detectable AC102 was present. Expression of AC102 was first detected at 12 hpi, and protein continued to accumulate through 36 hpi. The timing of AC102 expression matched that of VP39, the major capsid protein and a tightly regulated late factor (22).

To confirm the lack of detectable AC102 expression during the early phase of infection, prior to the initiation of DNA replication, infected cells were treated with aphidicolin, a drug that inhibits DNA synthesis and thus prevents the early-to-late transition. No AC102 was detected by Western blotting after aphidicolin treatment (Fig. 1B). These data indicate that *ac102* is predominantly expressed as a late gene.

The AC102-K66A mutation results in 10-fold-reduced viral titers and small plaques. Given that AC102 is predominantly expressed late in infection, we next sought to investigate the late function(s) of AC102. Because *ac102* is an essential gene (14, 23), cells transfected with the WOBpos-*Ac*Δ*102* bacmid do not produce progeny BV, precluding analysis of the roles of AC102 throughout viral replication. Therefore, we generated 10 mutant viruses carrying one of the following point mutations in AC102: N47A, T53A, A55V, D61A, K66A, S77A, A80V, L96A, L105A, or N114A. These amino acid residues were chosen because they are highly conserved between orthologs of AC102 in diverse alphabaculoviruses (Fig. 2). Growth of the mutants was initially assessed by infecting cells at an MOI of 10 and then measuring viral titer at 18 or 48 hpi (Table 1). One virus, containing the AC102-D61A mutation, did not produce any detectable progeny, suggesting this mutation causes inviability. Most other mutants exhibited modest 2- to 5-fold reductions in viral titer compared to WOBpos at one or both time points. The AC102-K66A mutant virus, in contrast, produced 10-fold-fewer BV progeny than WOBpos at both time points and was chosen for further analysis. In a more comprehensive one-step growth curve, the AC102-K66A mutant produced 10-fold-fewer progeny at 18, 24, 36, and 48 hpi (Fig. 3A, left). To assess whether the AC102-K66A mutation was the cause of the growth defect, an AC102-K66A-rescue virus was generated by inserting a wild-type copy of *ac102* into the bacterial replication cassette in the AC102-K66A bacmid (9). The growth kinetics of the AC102-K66A-rescue virus were indistinguishable from those of WOBpos (Fig. 3A, right). Thus, the AC102-K66A mutation causes a 10-fold reduction in BV progeny production throughout the late phase of infection.

In addition to the replication defect, the AC102-K66A mutant virus produced plaques that were 6-fold smaller than those produced by WOBpos or AC102-K66A-rescue (Fig. 3B). These small plaques typically consisted of only one or a few infected cells (Fig. 3C). The small plaques suggest that the AC102-K66A mutation results in a reduced capacity to spread from cell to cell.

The AC102-K66A mutation results in lower AC102 expression. To further investigate the nature of the defect caused by the AC102-K66A mutation, we compared the relative levels of wild-type AC102 and mutant AC102-K66A protein over the course of infection using Western blotting (Fig. 4A and B). For both, initial expression was

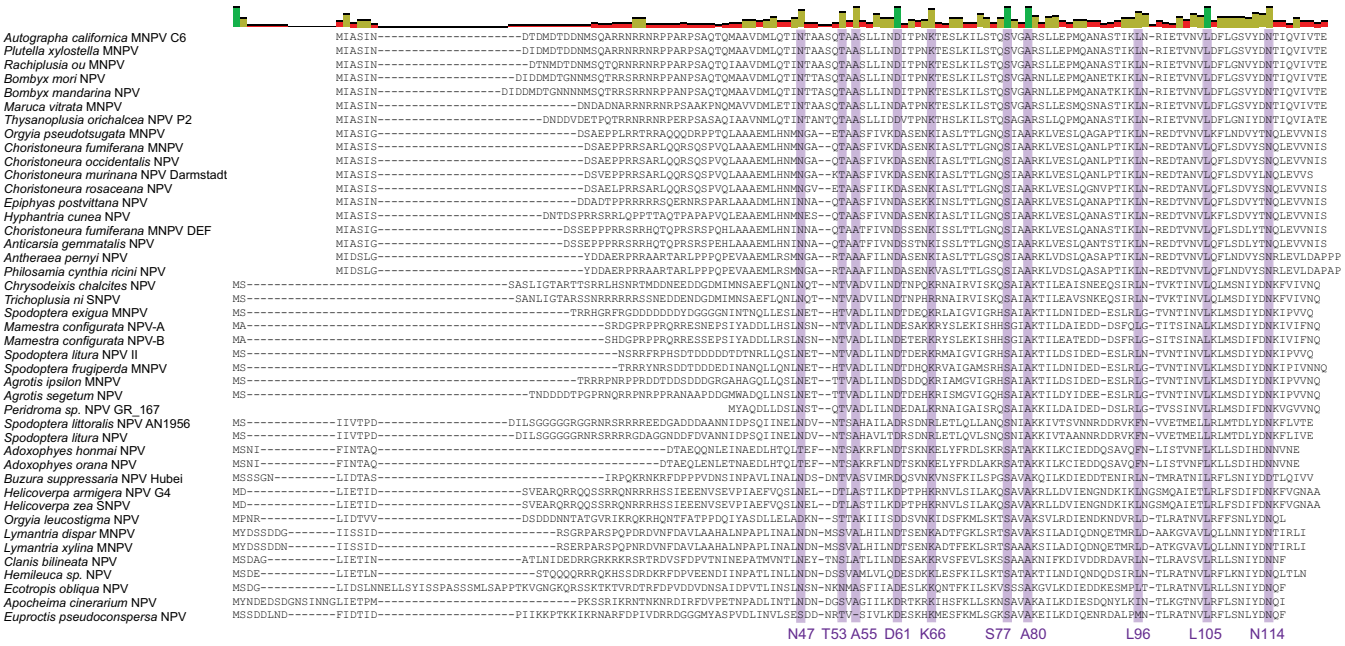

FIG 2 Alignment of AC102 protein sequences from alphabaculoviruses. AC102 amino acid sequences were aligned using MAFFT (56) and then manually edited for quality. Residues with at least 85% identity across all alphabaculoviruses are highlighted in purple.

observed at 12 hpi. However, at all time points tested, the levels of AC102-K66A were significantly reduced compared to wild-type AC102 (Fig. 4B). These results indicate that the AC102-K66A mutation does not affect the onset of AC102 expression but results in lower protein levels, probably by impacting the translation or stability of AC102.

We also observed the effect of the AC102-K66A mutation on the abundance and localization of AC102 in infected cells by immunofluorescence microscopy. At 12 hpi, AC102 was not visible in WOBpos-infected or AC102-K66A-infected cells (Fig. 4C and D). At 24 and 36 hpi, WOBpos-infected cells showed strong a AC102 signal in the nucleus, particularly in and around the VS (identified by a region of intense staining of viral DNA). In contrast, most AC102-K66A-infected cells showed reduced levels of AC102 in the nucleus with staining that was often limited to a thin outline of the VS at 24 and 36 hpi (Fig. 4C and D). Thus, the AC102-K66A mutation causes a reduction of AC102 and a redistribution to the periphery of the VS.

AC102 promotes a condensed virogenic stroma and is important for nucleocapsid assembly. To further elucidate the roles of AC102 in the nucleus, we examined the effect of the AC102-K66A mutation on nuclear organization and nucleocapsid

TABLE 1 Titers of the WOBpos wild-type virus and 9 *ac102* mutant viruses at 18 and 48 hpi[a]

Virus	Mean titer ± SD at:	
	18 hpi	48 hpi
WOBpos	$3.5 \times 10^5 \pm 0.4 \times 10^5$	$7.7 \times 10^7 \pm 0.3 \times 10^7$
AC102-N47A	$1.5 \times 10^5 \pm 0.4 \times 10^5$	$4.8 \times 10^7 \pm 0.5 \times 10^7$
AC102-T53A	$3.2 \times 10^5 \pm 0.3 \times 10^5$	$6.3 \times 10^7 \pm 1.3 \times 10^7$
AC102-A55V	$1.5 \times 10^5 \pm 0.1 \times 10^5$	$3.9 \times 10^7 \pm 0.2 \times 10^7$
AC102-K66A	$3.6 \times 10^4 \pm 0.7 \times 10^4$	$7.7 \times 10^6 \pm 1.0 \times 10^6$
AC102-S77A	$1.8 \times 10^5 \pm 0.1 \times 10^5$	$7.7 \times 10^7 \pm 0.4 \times 10^7$
AC102-A80V	$4.4 \times 10^5 \pm 0.6 \times 10^5$	$1.5 \times 10^7 \pm 0.2 \times 10^7$
AC102-L96A	$5.5 \times 10^4 \pm 1.0 \times 10^4$	$6.3 \times 10^7 \pm 0.3 \times 10^7$
AC102-L105A	$3.8 \times 10^5 \pm 0.5 \times 10^5$	$3.6 \times 10^7 \pm 0.1 \times 10^7$
AC102-N114A	$1.1 \times 10^5 \pm 0.3 \times 10^5$	$2.6 \times 10^7 \pm 0.2 \times 10^7$

[a]Cells were infected at an MOI of 10, and progeny virus released into the growth media 18 and 48 h postinfection (hpi) was enumerated by titer determinations. Experiments were performed in triplicate. AC102-D61A produced no viral progeny and thus could not be amplified for determination of titers.

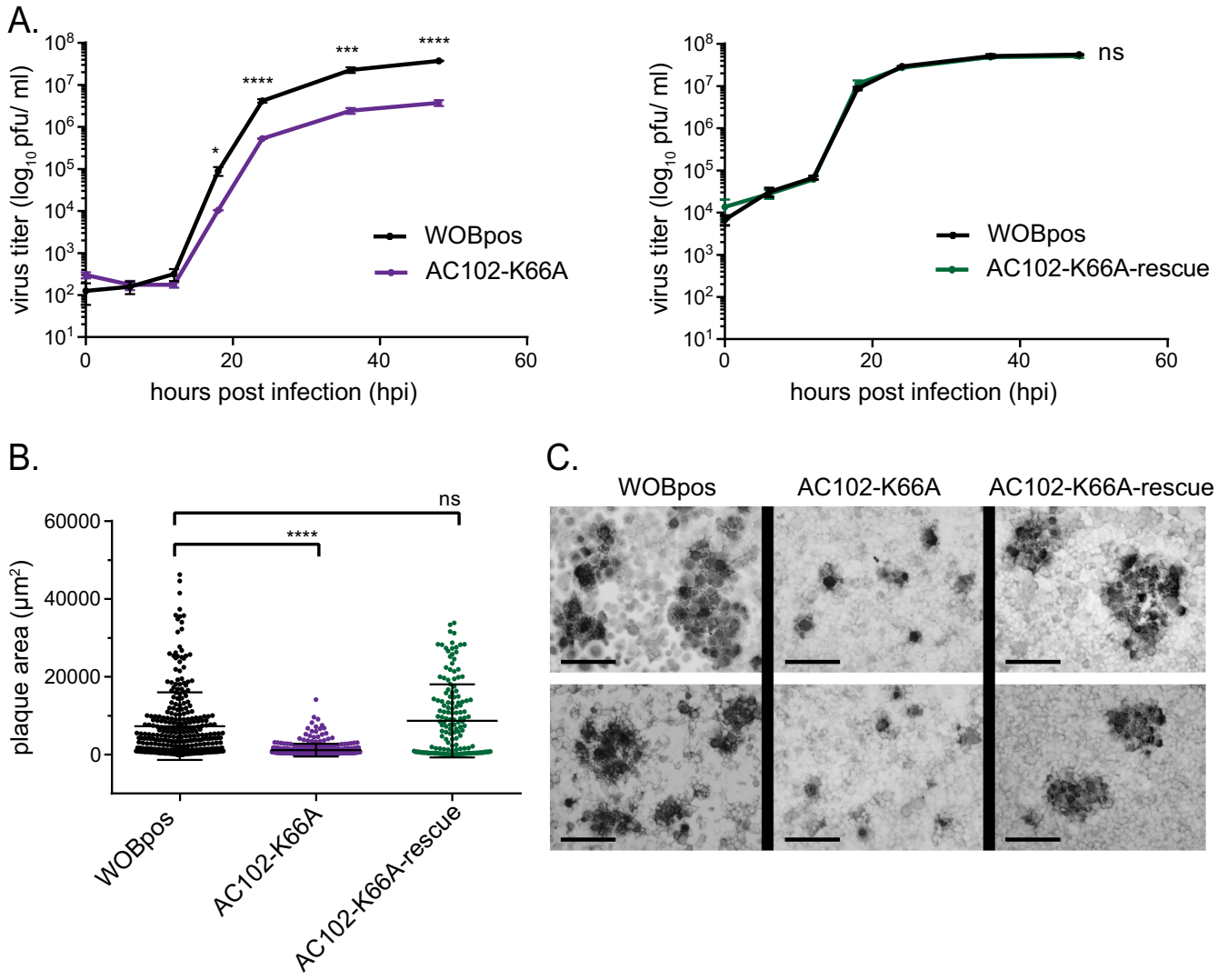

FIG 3 The AC102-K66A mutation results in 10-fold-reduced viral titers and a small plaque phenotype. (A) One-step growth curves of WOBpos and AC102-K66A viruses (left) or WOBpos and AC102-K66A-rescue viruses (right). Data are the means ± the standard deviations (SD) from three independent experiments. *P* values were calculated using a Student *t* test and are indicated as follows: ns, nonsignificant; *, $P < 0.05$; ***, $P < 0.001$; and ****, $P < 0.0001$. (B) Quantification of plaque area for WOBpos ($n = 303$), AC102-K66A ($n = 344$), AC102-K66A-rescue ($n = 160$). Each point represents one plaque size measurement, pooled from three independent experiments. The center bar represents the mean, and the top and bottom bars represent the SD. *P* values were calculated by a Kruskal-Wallis test, followed by a Dunn's posttest, and are indicated as follows: ns, nonsignificant; and ****, $P < 0.0001$. (C) Plaques resulting from WOBpos, AC102-K66A, or AC102-K66A-rescue viruses visualized by immunostaining for viral envelope protein GP64. Scale bars, 100 μm.

assembly. We initially noted that in AC102-K66A-infected cells, the VS appeared to be less condensed than that of WOBpos-infected cells, with the structure taking up almost the entire nucleus (Fig. 4D). To confirm the effect of AC102-K66A on the VS, we performed immunofluorescence microscopy using an antibody against PP31, a delayed early protein and VS marker (24). The timing of PP31 expression appeared to be similar in WOBpos-infected and AC102-K66A-infected cells (Fig. 5A and C). At 12 hpi, only dim PP31 signal could be detected in the nuclei of both AC102-K66A-infected and WOBpos-infected cells (Fig. 5A). At 24 and 36 hpi, PP31 was localized to the condensed VS in WOBpos-infected cells and to a less condensed VS in AC102-K66A-infected cells. At both time points, PP31 was also less abundant in the VS in AC102-K66A-infected cells compared to WOBpos-infected cells. These results confirm that the AC102-K66A mutation results in an aberrant and decondensed VS structure.

We also investigated the effect of AC102-K66A on the expression and localization of the major capsid protein VP39. As with PP31, the timing of VP39 expression appeared

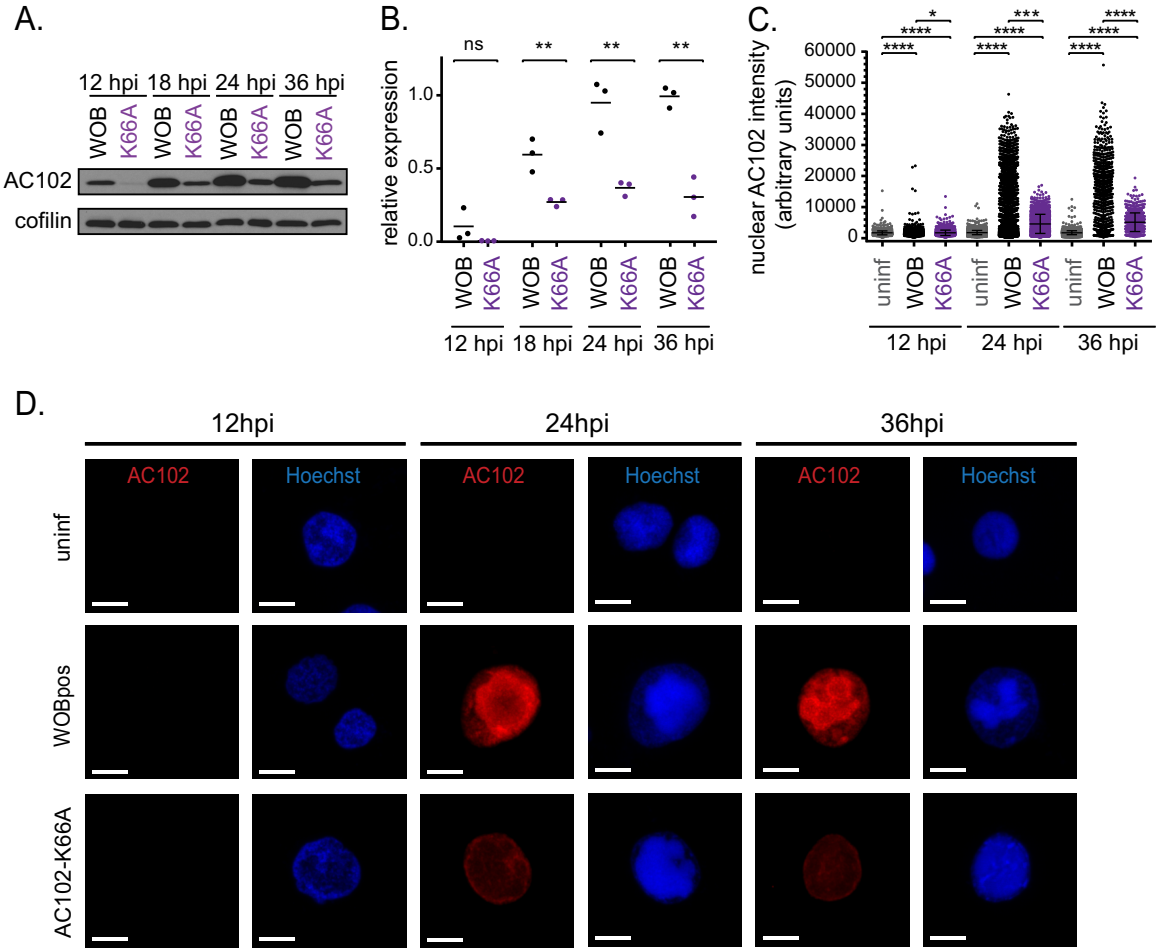

FIG 4 The AC102-K66A mutation results in lower AC102 expression and altered localization to the periphery of the virogenic stroma. (A) Western blot of lysates from Sf9 cells infected with WOBpos or AC102-K66A virus at an MOI of 10, prepared at 12, 18, 24, or 36 hpi, and probed for AC102 and cofilin (loading control). (B) Quantification of AC102 protein levels from Western blots by densitometry. Each dot represents the expression level in one independent experiment relative to the mean for WOBpos at 36 hpi. Lines indicate the means from three independent replicates. *P* values were calculated using a Student *t* test and are indicated as follows: ns, nonsignificant; and **, $P < 0.01$. (C) Nuclear intensity of AC102 immunofluorescence staining in uninfected Sf21 cells (uninf) or in cells infected with WOBpos or AC102-K66A virus at an MOI of 10 and fixed at 12, 24, or 36 hpi. Bars indicate the means from three independent replicates, and error bars indicate the SD. *P* values were calculated by the Kruskal-Wallis test, followed by a Dunn's posttest, and are indicated as follows: ns, nonsignificant; *, $P < 0.05$; ***, $P < 0.001$; and ****, $P < 0.0001$. (D) Sf21 cells stained for AC102 (immunofluorescence; red) and DNA (Hoechst; blue). Scale bars, 10 μm.

unaffected in the AC102-K66A mutant (Fig. 5B and D). At 12 hpi, VP39 showed punctate localization to the VS both in WOBpos-infected and AC102-K66A-infected cells (Fig. 5B). At 24 hpi, however, when WOBpos-infected cells continued to show punctate or diffuse VP39 localization in the VS, the majority of AC102-K66A-infected cells had VP39 in the RZ, where it often assembled into long filaments. At 36 hpi, VP39 redistributed to a punctate localization in the RZ in WOBpos-infected cells, whereas it remained filamentous in the ring zones of most AC102-K66A-infected cells. We quantified VP39 distributions in WOBpos-infected and AC102-K66A-infected cells by dividing cells into three phenotypic classes: (i) wild type with punctate distribution in the VS or RZ, (ii) "filamentous" with long thin filaments in the RZ, and (iii) "cable-like" with thick VP39 cables in the RZ (Fig. 5E). At 24 and 36 hpi, the majority of WOBpos-infected cells had wild-type VP39 distribution, whereas the majority of AC102-K66A-infected cells had a filamentous phenotype, and only AC102-K66A-infected cells contained cable-like VP39 structures. Thus, the AC102-K66A mutation causes aberrant assembly of VP39 into filamentous structures late in infection.

We used transmission electron microscopy (TEM) to further compare intranuclear structures in WOBpos-infected and AC102-K66A-infected cells. At 24 hpi, WOBpos-

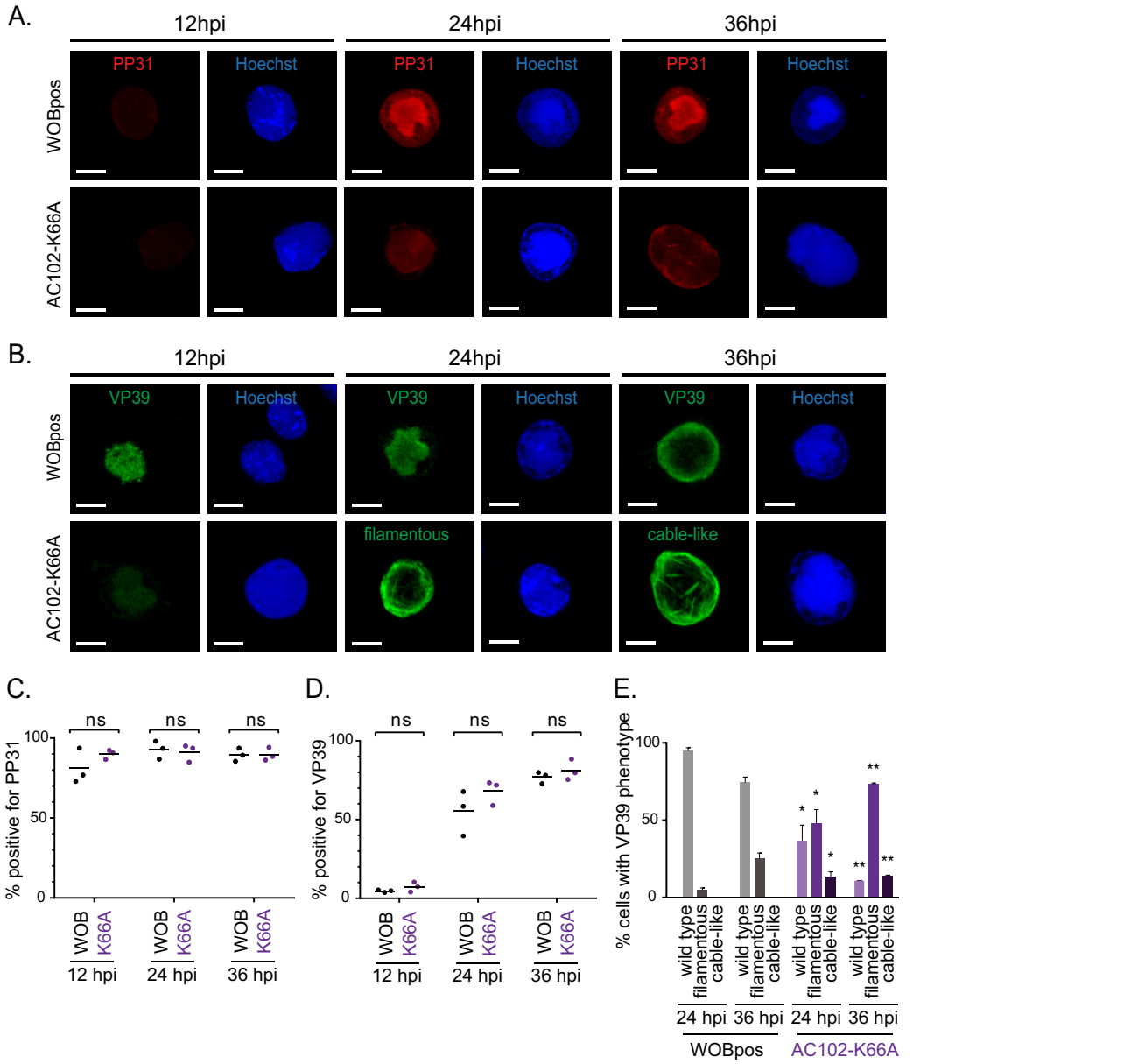

FIG 5 AC102 is important for the maintenance of a condensed virogenic stroma and for normal VP39 localization. (A) Sf21 cells infected with WOBpos or AC102-K66A at an MOI of 10, fixed at the indicated times postinfection, and stained for PP31 (immunofluorescence; red) and DNA (Hoechst; blue). (B) Sf21 cells infected with WOBpos or AC102-K66A at an MOI of 10, fixed at the indicated times, and stained for VP39 (immunofluorescence; green) and DNA (Hoechst; blue). Scale bars (panels A and B), 10 μm. (C and D) Quantification of the percentage of cells infected with WOBpos or AC102-K66A and fixed at the indicated times that express PP31 (C) or VP39 (D). Each dot represents the average percentage of cells positive for each marker for one independent experiment. Lines indicate the means from three independent replicates. Based on the Student *t* test, there were no significant differences (ns) at each time point tested. (E) Quantification of the percentage of cells infected with WOBpos or AC102-K66A, fixed at the indicated times, that exhibit each VP39 phenotype: "wild type," with punctate or diffuse VP39 distribution in the VS or RZ; "filamentous," with long and thin VP39 filaments localized in the RZ; and "cable-like," with thick VP39 cables localized in the RZ. Data are means ± the SD for two independent experiments, with 100 to 400 cells counted per experiment. *P* values were calculated using a Student *t* test by comparing like phenotypes between WOPpos and AC102-K66A at each time point and are indicated as follows: *, $P < 0.05$; and **, $P < 0.01$.

infected cells showed a condensed VS, composed of electron-dense lobes, and a peripheral RZ, both of which contained nucleocapsids (Fig. 6A and B). In contrast, AC102-K66A-infected cells lacked a well-defined VS, instead containing a more amorphous region that occupied most of the nucleus and did not contain electron-dense lobes or visible nucleocapsids (Fig. 6C). Moreover, in AC102-K66A-infected cells, the

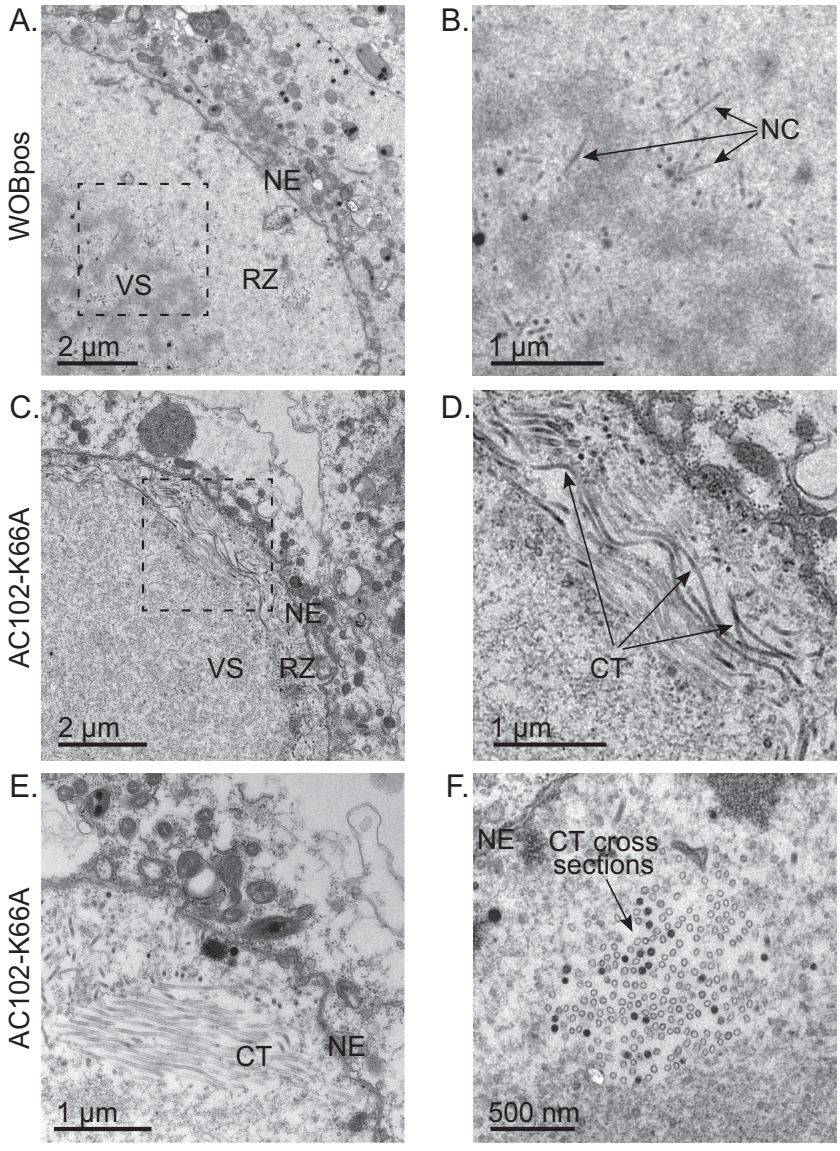

FIG 6 Electron microscopy confirms roles for AC102 in proper nucleocapsid morphogenesis and virogenic stroma formation. (A) Electron micrographs of Sf9 cells infected with WOBpos at an MOI of 10, fixed at 24 hpi, and prepared for TEM. The nuclear envelope (NE), ring zone (RZ), and virogenic stroma (VS) are indicated. (B) Magnified view of boxed area in panel A showing individual nucleocapsids (NC). (C) Electron micrographs of Sf9 cells infected with AC102-K66A, as in panel A. The nuclear envelope (NE), ring zone (RZ), and virogenic stroma (VS) are indicated. (D) Magnified view of boxed area in panel C showing capsid-like tubule structures (CT). (E and F) Electron micrographs of Sf9 cells infected with AC102-K66A, as in panel A, showing aggregates of capsid-like tubule structures (CT), in both a longitudinal section (E) and a cross section (F).

peripheral RZ was densely packed with long tubular structures that were variable in length and were often bundled or clustered (Fig. 6D to F). The tubules also varied in electron density, with some being nearly electron-lucent and others having electron-dense areas indicating the packaging of viral DNA (Fig. 6E and F). Taken together with the VP39 localization studies, these results suggest that the tubular structures are aberrant assemblies of VP39 that are not properly formed into unit-length nucleocapsids and are instead assembled into long tubular structures that sometimes contain viral DNA.

AC102 is crucial for nuclear actin polymerization in the ring zone late in infection. Our previous work suggested that AC102 is required for nuclear actin polymerization, since the transfection of cells with a WOBpos bacmid carrying a

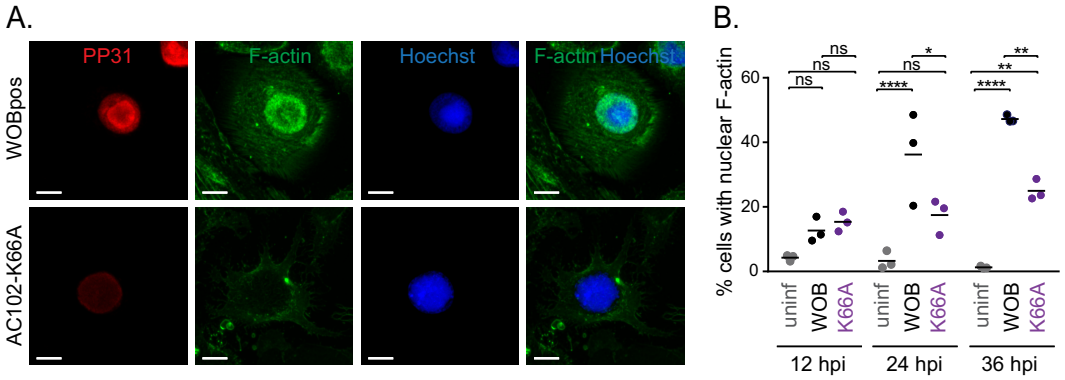

FIG 7 AC102 is crucial for nuclear actin polymerization in the ring zone during late infection. (A) Sf21 cells infected with WOBpos or AC102-K66A virus at an MOI of 10, fixed at 36 hpi, and stained for PP31 (immunofluorescence; red), F-actin (Alexa Fluor-phalloidin; green), and DNA (Hoechst; blue). Scale bars, 10 μm. (B) Quantification of the percent cells with nuclear F-actin at 12, 24, and 36 hpi, defined as cells with a nuclear/cytoplasmic F-actin intensity ratio of 2 or greater, from Alexa Fluor 488-phalloidin staining. Each dot represents the average percentage of cells containing nuclear actin for one independent experiment. Lines indicate the means for three independent experiments. *P* values were calculated by one-way analysis of variance, followed by an Šídák posttest, and are indicated as follows: ns, nonsignificant; *, $P < 0.05$; **, $P < 0.01$; and ****, $P < 0.0001$.

deletion of *ac102* (*AcΔ102*) caused a failure in nuclear F-actin accumulation (14). However, the *AcΔ102* virus does not complete a replication cycle and thus does not necessarily capture the roles of AC102 during the course of a viral infection. To further investigate the role of AC102 in nuclear actin polymerization, we tested the ability of the AC102-K66A virus to cause nuclear accumulation of F-actin late in infection by fluorescence microscopy (Fig. 7A). A considerable fraction of WOBpos-infected cells contained nuclear F-actin (defined as a nuclear/cytoplasmic actin intensity ratio of 2 or greater) at 24 and 36 hpi, whereas substantially fewer AC102-K66A-infected cells exhibited nuclear F-actin accumulation at these time points (Fig. 7B). These results confirm that AC102 is important for nuclear actin polymerization late in infection.

The AC102-K66A mutation results in a defect in polyhedrin expression and polyhedra formation. We also investigated a possible function for AC102 very late in infection by assessing the timing and expression of the very late protein polyhedrin in WOBpos-infected and AC102-K66A-infected cells by Western blotting (Fig. 8A and B). At 18 hpi, there was no detectable expression of polyhedrin, as expected for a very late protein. At 24 hpi, WOBpos-infected cells showed strong expression of polyhedrin, whereas AC102-K66A-infected cells showed very little expression. At 36 hpi, polyhedrin expression was significantly higher in WOBpos-infected cells than in AC102-K66A-infected cells. To assess whether lower polyhedrin expression also correlated with fewer polyhedra, we imaged infected cells at 36 hpi using TEM and counted the fraction with at least one polyhedron (Fig. 8C and D). Compared to WOBpos-infected cells, significantly fewer AC102-K66A-infected cells contained polyhedra. Together, these data indicate that perturbing AC102 function impacts the proper timing of polyhedrin expression and the formation of polyhedra during the transition to very-late-stage infection.

AC102 is a nucleocapsid protein that interacts with P78/83, C42, and EC27. The timing of AC102 expression as a late gene and the effect of the AC102-K66A mutation on nucleocapsid morphogenesis suggested that AC102 may be a structural component of the nucleocapsid. To test whether AC102 is a virion-associated protein, BV particles were isolated via ultracentrifugation over a sucrose cushion and then fractionated into their envelope and nucleocapsid components. Western blotting revealed that AC102 is associated with the nucleocapsid fraction, but not with the envelope fraction (Fig. 9A). These results indicate that AC102 is a structural component of nucleocapsids.

As a nucleocapsid structural component, AC102 would be predicted to interact with other capsid proteins. To identify the specific viral proteins with which AC102 interacts,

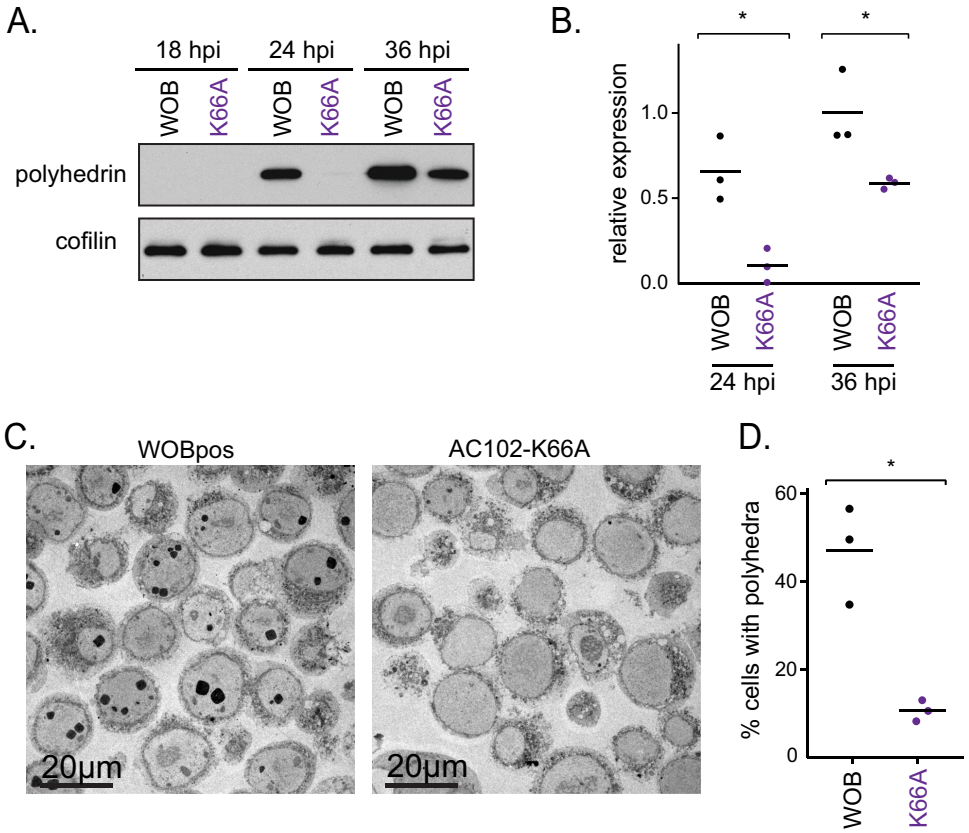

FIG 8 AC102 is important for polyhedrin expression and polyhedrin formation very late in infection. (A) Western blots of lysates from Sf9 cells infected with WOBpos at an MOI of 10 and probed at 18, 24, or 36 hpi for polyhedrin (top) or cofilin (loading control). (B) Quantification of AC102 protein levels from Western blots. Each dot represents the expression level relative to the mean for WOBpos at 36 hpi in one independent experiment. Lines are the mean from three independent replicates. *P* values were calculated using a Student *t* test and are indicated as follows: *, $P < 0.05$. (C) TEM images of WOBpos-infected or AC102-K66A-infected cells at 36 hpi showing the presence or absence of electron-dense polyhedra. (D) Percentages of cells with at least one polyhedra for WOBpos-infected or AC102-K66A-infected cells visualized as in panel C. Each dot represents the average percentage of cells with at least one polyhedra for one independent experiment, and lines indicate the means for three independent experiments. *P* values were calculated using Student *t* test and are indicated as follows: *, $P < 0.05$.

a virus was constructed that expresses AC102 fused to a Twin-Strep-tag (25) in the native *ac102* locus of the viral genome. The AC102-Strep virus grows at a rate that is indistinguishable from WOBpos (Fig. 9B), indicating that the AC102-Strep protein is fully functional. To purify AC102 with interacting proteins, Sf9 cells were infected with AC102-Strep or WOBpos as a control, and at 24 hpi cells were lysed and AC102-Strep protein was isolated by Strep-Tactin affinity chromatography. Interestingly, AC102-Strep copurified with three prominent viral proteins that were identified by SDS-PAGE and mass spectrometry of isolated gel bands as EC27, C42, and P78/83 (Fig. 9C), which were previously found to interact with one another in a complex (17). Furthermore, comparative mass spectrometry of AC102-Strep elution samples revealed that AC102, and these three proteins were the most abundant viral proteins in the pulldown (Table 2). Other less abundant proteins identified in the pulldown (E25, E18, VP39, and VP80) were also identified as virion-associated proteins by mass spectrometry (26–28). Taken together, these results indicate that AC102 is a nucleocapsid protein that interacts in a complex with the other nucleocapsid proteins P78/83, C42, and EC27.

DISCUSSION

AcMNPV protein AC102 was previously shown to be essential for viral replication (14, 23), sufficient to induce nuclear localization of actin (NLA) when expressed with five other viral NLA genes (13), and necessary for NLA (14). Although AC102 was proposed

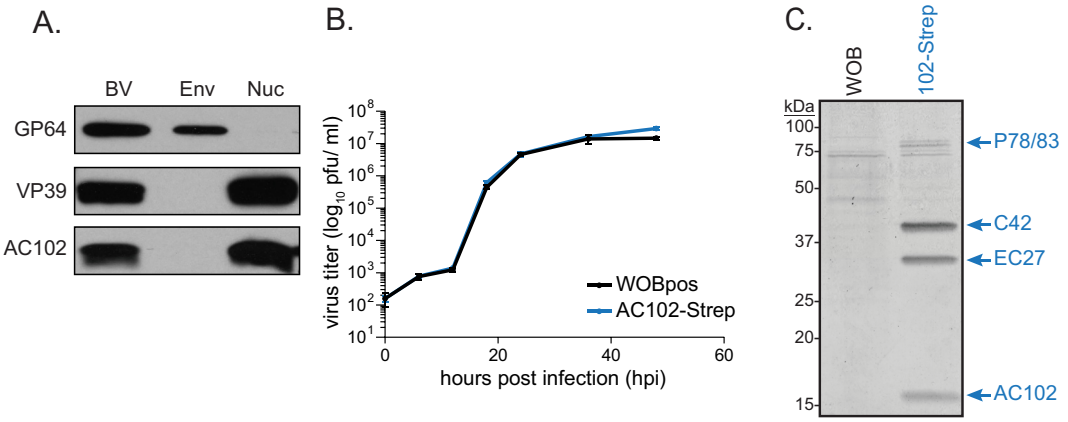

FIG 9 AC102 is a nucleocapsid protein that interacts with P78/83, C42, and EC27. (A) Western blots of total budded virus (BV), envelope (Env), and nucleocapsid fractions (Nuc) probed for GP64 (envelope control), VP39 (nucleocapsid control), and AC102. (B) One-step growth curves of WOBpos and AC102-Strep viruses in Sf9 cells infected at an MOI of 10. Data are means ± the SD from three independent experiments. (C) Strep-Tactin-affinity chromatography eluates from WOBpos-infected and AC102-Strep-infected Sf9 cell lysates at 24 hpi. Equal amounts of sample were subjected to SDS-PAGE, the gel was stained with Safestain, and bands that were unique to the AC102-Strep sample were excised and analyzed by mass spectrometry. The protein identity of each band is indicated.

to be expressed early in infection based on its role in NLA (13), we reveal here a role for AC102 as a late-expressed nucleocapsid protein that is a component of the P78/83-C42-EC27-AC102 complex and is crucial for VS organization, nucleocapsid morphogenesis, and nuclear F-actin assembly.

Our findings demonstrate that AC102 is expressed predominantly late in infection, with detectable protein first observed at 12 hpi. The onset of AC102 expression is consistent with the onset of *ac102* mRNA accumulation, which begins at 12 hpi and peaks at 18 hpi based on transcriptomics studies (21). AC102 protein levels continue to accumulate through at least 36 hpi, suggesting that mRNA and protein levels may not be directly correlated at later time points. The onset of AC102 expression is similar to that of VP39, which is strictly expressed late in infection (22). Furthermore, AC102 expression is undetectable after treating cells with aphidicolin, which prevents late gene expression. Thus, *ac102* is predominantly expressed as a late gene.

Many late viral proteins are structural components of virions, and our data indicate that AC102 associates with BV nucleocapsids but not with their envelopes. Furthermore, we find that AC102 interacts in a complex with the nucleocapsid proteins P78/83, C42, and EC27, which were previously shown to interact with one another (17). AC102 had not, however, been recognized as a member of this complex. The associations

TABLE 2 Mass spectrometry results from Strept-Tactin-affinity chromatography eluates

Protein	Accession no.	Normalized abundance[a]				Protein spectral counts/total spectral counts[d]			
		AC102-Strep	Control	*P*[b]	HGSCore[c]	AC102-Strep 1	AC102-Strep 2	Control 1	Control 2
C42	P25695	3.64	0.03	0.0002	7.417	2,010/26,093	3,058/30,523	21/6,511	26/6,785
EC27	P41702	1.94	0.03	0.0002	7.722	1,019/26,093	1,152/30,523	15/6,511	18/6,785
P78/83	Q03209	1.10	0.03	0.0001	7.868	1,227/26,093	1,074/30,523	28/6,511	33/6,785
AC102	P41482	1.00	0.02	*	N/A	227/26,093	244/30,523	6/6,511	4/6,785
E25	P41483	0.98	0.52	0.0008	5.583	345/26,093	514/30,523	237/6,511	225/6,785
E18	P41701	0.90	0.17	0.002	4.631	78/26,093	233/30,523	34/6,511	24/6,785
VP39	P17499	0.55	0.09	0.006	1.888	309/26,093	434/30,523	65/6,511	56/6,785
VP80	Q00733	0.27	0.02	0.020	0.354	334/26,093	398/30,523	18/6,511	26/6,785

[a]Normalized abundance was calculated by dividing the number of spectral counts by the protein amino acid length to determine the relative abundance and then dividing the relative abundance of each protein by the relative abundance of AC102. Positive protein hits are ranked by normalized abundance.
[b]*P* values were calculated using the Spotlite web application with the HGSCore scoring algorithm. The asterisk indicates a value of 1, since protein abundance was normalized to AC102.
[c]A higher HGSCore means a higher probability of protein-protein interactions.
[d]Numbers are given for two independent replicates from Strep-Tactin affinity eluates from both AC102-Step and control lysates.

between P78/83, C42, and EC27 were discovered through yeast two-hybrid studies, which rely on the interaction of bait and prey proteins fused with domains from a transcription factor. We have found that AC102 is not functional when fused at its N or C terminus with larger proteins (unpublished observations), offering a possible explanation as to why interactions with AC102 may have been missed in two-hybrid assays.

A previous analysis of AC102 function relied on the characterization of an *AcΔ102* mutant following bacmid transfection, which does not result in the production of viral progeny (14), thus precluding a thorough assessment of the role of AC102 throughout infection. Our characterization of the AC102-K66A partial loss-of-function mutant virus alleviates this issue and has revealed new roles of AC102 during late infection. We found that AC102 is important for establishing and/or maintaining a condensed VS, as this structure was expanded and amorphous in AC102-K66A-infected cells. This is similar to what has been seen in cells treated with cytochalasin D (10), a drug that inhibits actin polymerization and also induces proteolysis of the genome packaging protein p6.9 (29). AC102 is also important for nucleocapsid morphogenesis, as aberrant capsid-like tubular structures accumulated in the RZ of AC102-K66A-infected cells as visualized by TEM. Similar tubular structures have been observed in cells treated with cytochalasin D (10, 30), as well as in cells transfected/infected with mutant bacmids/viruses carrying deletions of *ac101/c42* and *ac144/ec27* (20), and other genes important for nucleocapsid assembly, including *vlf-1/ac77* (31), *49K/ac142* (20), *38K/ac98* (32), *ac54* (33, 34), *ac53* (35), and *pk-1/ac10* (36). These aberrant tubular structures contain the major capsid protein VP39 (20, 30, 32) and are thought to result from perturbed nucleocapsid assembly. The presence of these structures is consistent with our immunofluorescence microscopy images showing VP39 mislocalized into filaments and cables in the RZ of AC102-K66A-infected cells. Taken together, these data confirm that AC102 is important for the proper organization of viral replication structures and nucleocapsid morphogenesis, most likely due to its role as a structural component of nucleocapsids.

Our observations indicate that, in cells infected with the AC102-K66A mutant, expression of the very late protein polyhedrin is also delayed and reduced, and fewer infected cells contain polyhedra compared to WOBpos-infected cells. This phenotype is similar to that recently observed for a virus carrying a point mutation in VP39 (VP39-G276S), which exhibits reduced expression of polyhedrin and fewer polyhedra (37). It was suggested that lower polyhedrin expression in the VP39-G276S mutant might result from the sequestration of viral DNA in aberrant tubular nucleocapsid-like structures, reducing transcription of viral genes, and a similar phenomenon may account for the phenotype of the AC102-K66A mutant.

Consistent with observations from cells transfected with an *AcΔ102* mutant bacmid (14), we also observed decreased levels of nuclear F-actin in late-stage AC102-K66A-infected cells. AC102's association with the P78/83-containing complex suggests a mechanism through which AC102 may impact actin polymerization in the nucleus. P78/83 is a viral protein that mimics host WASP family proteins (16) and activates the host Arp2/3 complex to promote actin polymerization (9). It is required for both actin-based motility during early infection (12) and nuclear F-actin polymerization during late infection (9). The defect in nuclear actin polymerization seen for the AC102-K66A mutant virus could therefore be caused by perturbed stability, localization or actin polymerization activity of the P78/83-C42-EC27-AC102 complex. Consistent with this notion, deletion of *c42/ac101* also causes a reduction in nuclear F-actin (38). Furthermore, because nuclear F-actin is required for progeny production (7–11), the reduced nuclear F-actin accumulation caused by the AC102-K66A mutation may in part account for reduced production of BV.

Interestingly, apart from their late functions, components of the P78/83-C42-EC27-AC102 complex have also been suggested to have functions early in infection. For example, AC102 activity in NLA can occur in the absence of late gene expression and requires prior expression of the viral early transcriptional activator IE1, as well as PE38 and AC152 (13), suggesting that these other NLA factors might regulate AC102 expres-

sion or activity early in infection to promote the nuclear localization of G-actin prior to its polymerization into F-actin. Moreover, C42 is reported to have other functions, including a role in the nuclear import of P78/83 (39). How early activity might occur remains unclear, since *p78/83*, *c42/ac101*, *ec27/ac144*, and *ac102* are predominantly late genes based on transcriptomics data (21). Nevertheless, these same data indicate that low levels of mRNA of all four genes are present 1 h after a viral inoculum was added to the cells (21), suggesting the possibility of early expression at low levels. Alternatively, the dose of these structural proteins delivered with the initial viral inoculum may be sufficient to carry out early functions.

In closing, our work reveals that AC102 is a central player that links the early nuclear accumulation of G-actin with later nuclear F-actin assembly and nucleocapsid morphogenesis. Future studies into the mechanistic roles of AC102 will reveal how it contributes to the regulation and activity of the P78/83-C42-EC27-AC102 complex and how it acts in nucleocapsid morphogenesis and the dramatic relocalization and polymerization of actin into the nucleus during baculovirus infection. Given our relatively limited understanding of the normal regulation and function of nuclear actin in uninfected cells, future studies of AC102 will also enhance our understanding of the diverse cellular functions of actin.

MATERIALS AND METHODS

Cell lines and viruses. Sf9 cells were maintained in ESF921 media (Expression Systems) at 28°C in shaker flasks. Sf21 cells were maintained in Grace's insect media (Gemini Bio-Products) with 10% fetal bovine serum and 0.1% Pluronic F-68 (Invitrogen) at 28°C in shaker flasks. AcMNPV WOBpos (9) was used as the wild-type virus in this study.

Generation of recombinant viruses. To generate viruses with point mutations in *ac102*, we first generated transfer vectors carrying the AcMNPV viral fragment KpnI-E (2.0 kb KpnI fragment of PstI-C containing *ac102* [13]) and a downstream chloramphenicol resistance (*cat*) cassette for later use in recombinant bacmid selection. These were cloned into the KpnI site of pBSKS+ (Agilent Technologies). A QuikChange II site-directed mutagenesis kit (Agilent Technologies) was used according to the manufacturer's protocol to produce 10 mutant transfer vectors encoding AC102 with one of the following point mutations: N47A, T53A, A55V, D61A, K66A, S77A, A80V, L96A, L105A, and N114A. To generate mutant viruses, *E. coli* strain GS1783 (40) (provided by Laurent Coscoy, University of California, Berkeley) was transformed with WOBpos viral DNA carrying a deletion of *ac102* (*AcΔ102*) (14). Transformed cells were shifted to 42°C for 15 min to express recombinase proteins and then electroporated with linearized mutant transfer vectors. Recombinant bacmids were selected by plating transformed cells on Luria-Bertani (LB) medium containing chloramphenicol and kanamycin. To generate the AC102-K66A-rescue virus, the transfer vector pAC102-rescue was engineered by amplifying *ac102* and its native promoter from viral DNA using PCR and then subcloning it into pWOBGent3 (12). *E. coli* strain GS1783 containing the AC102-K66A mutant bacmid was shifted to 42°C as described above and then electroporated with linearized pAC102-rescue DNA. Recombinant bacmids were selected by plating transformed cells on LB medium containing gentamicin. This resulted in one copy of *ac102* under the control of its native promoter being inserted into the AC102-K66A bacmid just upstream of the kanamycin resistance cassette. To generate the AC102-Strep virus, the transfer vector pAC102-StrepII was engineered by amplifying a gene encoding AC102 tagged with a Twin-Strep-tag (25). *E. coli* strain GS1783 containing the *AcΔ102* bacmid (14) was shifted to 42°C as described above and then electroporated with linearized pAC102-StrepII DNA. This resulted in the insertion of the *ac102-Strep* gene into the native *ac102* locus. Recombinant bacmids were selected for by plating transformed *E. coli* onto LB plates containing chloramphenicol. In all cases, isolated bacmid DNA was transfected into Sf9 cells using TransIT-Insect transfection reagent (Mirus Bio LLC), and virus was recovered from transfected cell supernatants. For all recombinant viruses, we confirmed proper homologous recombination and the presence of *ac102* point mutations by restriction endonuclease digestion analysis of viral DNA, as well as by PCR and DNA sequencing.

Viral growth curves and plaque size measurements. To compare the kinetics of progeny BV production for WOBpos, AC102-K66A, AC102-K66A-rescue, and AC102-Strep viruses, one-step growth curves were performed in triplicate using an immunoplaque assay (41). To measure plaque size, images of plaques were captured on an Olympus IX71 microscope with a ×20 objective lens (Olympus LUCPlanFL, 0.45 NA), a CoolSNAP HQ camera (Photometrics), and μManager software (42). The Fiji distribution of ImageJ (43) was used to measure the area of individual plaques.

BV purification and fractionation. To obtain purified BV, Sf9 cells were infected with WOBpos at a multiplicity of infection (MOI) of 10, and cell culture supernatant containing BV was collected at 2 days postinfection. The supernatant was then overlaid onto a 40% sucrose cushion and centrifuged at 100,000 × *g* for 1 h at 15°C using a Beckman SW-28 rotor in a Beckman L8-M ultracentrifuge to pellet BV particles. BV was then resuspended in 10 mM Tris buffer (pH 8.5). To further fractionate BV into envelope and nucleocapsid components, NP-40 was added to 100 μg of BV at a final concentration of 1%, incubated for 1 h at 4°C, and the sample was centrifuged at 80,000 × *g* for 1 h at 15°C using a Beckman TLA-100 rotor in a Beckman TL-100 ultracentrifuge to separate the supernatant fraction containing viral envelope proteins from the pellet fraction containing nucleocapsid-associated proteins. The nucleocapsid fraction

was then washed and centrifuged a second time under identical conditions to ensure that there was no contamination from the envelope fraction.

Purification and identification of AC102 interacting proteins. To purify AC102-Strep together with interacting proteins, Sf9 cells were infected with AC102-Strep or control WOBpos viruses at an MOI of 10, and infected cells were harvested at 24 hpi. Cells were lysed on ice for 10 min in lysis buffer (50 mM Tris-HCl, 150 mM NaCl, 1 mM EDTA, 1% Triton X-100, 1 μg/ml each leupeptin, pepstatin, and chymostatin (LPC), 1 μg/ml aprotinin, and 1 mM phenylmethylsulfonyl fluoride [PMSF]) and centrifuged in a microcentrifuge at 16,000 $\times$ *g* for 2 min at room temperature to separate nuclei and cellular debris from the cytoplasmic supernatant. The clarified cell lysate was incubated with 50 μl (packed volume) of Strep-Tactin Sepharose resin (IBA Lifesciences) for 2 h at 4°C with rotation. Beads were washed with lysis buffer containing 300 mM NaCl, and protein was eluted with lysis buffer containing 6 μM D-desthiobiotin (IBA Lifesciences). The protein concentration was assessed using a Bradford assay. Samples containing equal amounts of protein were separated by SDS-PAGE, and gels were stained with SimplyBlue SafeStain (Thermo Fisher Scientific) according to the manufacturer's maximum-sensitivity protocol.

For identification of individual proteins visualized by SDS-PAGE, bands that were unique to the AC102-Strep pulldown were cut out, in-gel digested with trypsin (44), and subjected to mass spectrometry as described below. In addition, for the bulk identification of eluted proteins, whole elution samples from three independent affinity chromatography experiments for both AC102-Strep and control WOBpos were trypsin digested and subjected to mass spectrometry as described below.

Mass spectrometry was performed by the Vincent J. Coates Proteomics/Mass Spectrometry Laboratory at the University of California, Berkeley. For whole elution samples, a nano-LC column consisting of 10 cm of Polaris C18 (5 μm; Agilent Technologies), followed by 4 cm of Partisphere 5 SCX (GE Healthcare Life Sciences), was washed extensively with buffer A (5% acetonitrile, 0.02% heptafluorobutyric acid [HBFA]). The column was then directly coupled to an electrospray ionization source mounted on a Thermo-Fisher LTQ XL linear ion trap mass spectrometer. An Agilent 1200 HPLC delivering a flow rate of 300 nl/min was used for chromatography. Peptides were eluted using an eight-step MudPIT procedure (45). The following buffers were used: buffer A (see above), buffer B (80% acetonitrile, 0.02% HBFA), buffer C (250 mM ammonium acetate, 5% acetonitrile, 0.02% HBFA), and buffer D (500 mM ammonium acetate, 5% acetonitrile, 0.02% HBFA). This protocol was also followed for proteins originating from gel bands, except that the nano-LC column was packed with 10 cm of Polaris C18 (5 μm) only, and the chromatography consisted of a simple gradient from 100% buffer A to 40% buffer A and 60% buffer B.

Protein identification and quantification were done with Integrated Proteomics Pipeline IP2 software (Integrated Proteomics Applications) using ProLuCID/Sequest (46), DTASelect (47, 48), and Census (49). Tandem mass spectra were extracted into ms1 and ms2 files from raw files using RawExtractor (50). Data were searched against the AcMNPV (NC_001623.1) translated protein database, supplemented with sequences of common contaminants, and concatenated to a decoy database in which the sequence for each entry in the original database was reversed (51). Linear trap quadropole (LTQ) data were searched with a 3,000.0-milli-amu precursor tolerance, and the fragment ions were restricted to a 600.0-ppm tolerance. All searches were parallelized and searched on the VJC proteomics cluster. Search space included all fully tryptic peptide candidates with no missed cleavage restrictions. Carbamidomethylation (+57.02146) of cysteine was considered a static modification. We required one peptide per protein and both tryptic termini for each peptide identification. The ProLuCID search results were assembled and filtered using the DTASelect program with a peptide false discovery rate (FDR) of 0.001 for single peptides and an FDR of 0.005 for additional peptides for the same protein. The estimated FDR was about 1% for the data sets used. To better distinguish direct from indirect interactions in whole elution samples, we used Spotlite (52), a web-based platform designed to identify specific protein-protein interactions from affinity purified samples subjected to mass spectrometry. We used the HGSCore scoring algorithm (53) within Spotlite to identify high-confidence interactions with a *P* value of <0.05.

AC102 purification and anti-AC102 antibody generation. To express recombinant AC102 protein, *ac102* was amplified by PCR and subcloned into the SspI site of pET-1M (provided by the University of California, Berkeley, QB3 MacroLab) to generate plasmid pET-1M-AC102 that encodes a fusion protein of AC102 with an N-terminal 6×His tag, maltose-binding protein (MBP), and tobacco-etch virus protease cleavage site (His-MBP-TEV-AC102). *E. coli* strain BL21(DE3) (New England BioLabs) was transformed with pET-1M-AC102, grown at 37°C to an optical density of 0.6 to 0.8, induced with 250 μM IPTG (isopropyl-β-D-thiogalactopyranoside) for 2 h, and then harvested. *E. coli* were resuspended in lysis buffer (100 mM Tris-HCl [pH 8.0], 150 mM NaCl, 1 mM EDTA, 1 μg/ml LPC, 1 μg/ml aprotinin, and 1 mM PMSF) and lysed by sonication, and lysates were centrifuged at 20,000 $\times$ *g* for 20 min at 4°C using an SS34 rotor in a Sorval RC5C Plus centrifuge. Clarified lysates were incubated with 10 ml (packed volume) of amylose resin (New England BioLabs) for 2 h at 4°C with rotation, washed with 10 volumes of column buffer (100 mM Tris-HCl [pH 8.0], 300 mM NaCl, 1 mM EDTA), and then eluted with column buffer containing 10 mM maltose. Protein-containing fractions were pooled, and MBP was cleaved from AC102 using 1 mg/ml TEV protease. Released His-MBP and uncleaved His-MBP-TEV-AC102 were removed by binding to HisPur Ni-NTA resin (Thermo Fisher Scientific). Purified AC102 was concentrated to 1 mg/ml with a 3-kDa-molecular-mass cutoff protein concentrator (Thermo Fisher Scientific).

To generate custom antibodies that recognize AC102, rabbits were immunized with the purified AC102 protein by Pocono Rabbit Farm and Laboratory, using their standard 91-day protocol. For antibody affinity purification, purified and concentrated AC102 was further purified via ion-exchange chromatography, using a HiTrap SP HP 1-ml column (GE Healthcare Life Sciences) and coupled to NHS-activated Sepharose 4 Fast Flow resin (GE Healthcare Life Sciences). Anti-AC102 serum was passed over the AC102 affinity resin, and antibodies were eluted with 100 mM glycine (pH 2.5). Antibodies were

immediately neutralized to pH 7.5 by adding 1 M Tris (pH 8.8) and stored at −20°C or −80°C in 50% glycerol.

Analysis of AC102 and AC102-K66A expression by Western blotting. To observe AC102 protein expression over the course of infection, Sf9 cells were infected in triplicate with WOBpos at an MOI of 10, and infected cells were harvested at 0, 8, 10, 12, 14, 16, and 36 hpi. Cells were lysed on ice for 10 min in lysis buffer (50 mM Tris-HCl [pH 8.0], 150 mM NaCl, 1 mM EDTA, 1% Triton X-100, 1 μg/ml LPC, 1 μg/ml aprotinin, and 1 mM PMSF) and centrifuged in a microcentrifuge at 16,000 $\times$ *g* for 2 min at room temperature to separate nuclei and cellular debris from the cytoplasmic supernatant. Cell lysates were subjected to SDS-PAGE, with equal loading of total protein in all lanes (as determined by a Bradford assay). Proteins were transferred to nitrocellulose membranes and probed by Western blotting with rabbit anti-AC102, mouse anti-VP39 antibody P10C6 (54) (kindly provided by JaRue Manning) and rabbit anti-cofilin antibody GA15 as a loading control (kindly provided by Michael Goldberg and Kris Gunsalus). To assess whether AC102 is expressed late in infection after the onset of DNA replication, cells were infected as described above in the presence of either 5 μg/ml aphidicolin or dimethyl sulfoxide (DMSO; as a control). At 24 hpi, cells were lysed and subjected to SDS-PAGE and Western blotting as described above using rabbit anti-AC102 and rabbit anti-cofilin antibodies.

To compare expression levels of AC102 and other proteins in WOBpos-infected and AC102-K66A-infected cells, Sf9 cells were infected in triplicate as described above and lysed at 0, 6, 12, 18, 24, and 36 hpi. Cell lysates were prepared and subjected to SDS-PAGE and Western blotting as described above using rabbit anti-AC102 antibody, rabbit anti-polyhedrin antibody (55) (generously provided by Loy Volkman), and rabbit anti-cofilin antibody.

Immunofluorescence microscopy. For immunofluorescence microscopy, Sf21 cells were seeded onto CELLSTAR black-walled 96-well plates with microclear bottoms (Grenier Bio-One) to ~75% confluence and infected in triplicate with WOBpos or AC102-K66A virus at an MOI of 10. At 12, 24, or 36 hpi, cells were fixed with 4% paraformaldehyde in PHEM buffer (60 mM PIPES [pH 6.9], 25 mM HEPES, 10 mM EGTA, 2 mM $MgCl_2$), permeabilized in PHEM with 0.15% Triton X-100, blocked in PHEM with 5% normal goat serum (MP Biomedicals) plus 1% bovine serum albumin, and processed for immunofluorescence staining as described previously (14). Primary antibodies used were: anti-AC102 at a 1:500 dilution in PHEM buffer, anti-VP39 P10C6 at a 1:200 dilution, or rabbit-anti-PP31 at a 1:200 dilution (24) (kindly provided by Linda Guarino). Phalloidin conjugated to Alexa Fluor 488 or Alexa Fluor 568 at a 1:400 dilution in PHEM buffer (Molecular Probes) was used to visualize F-actin, and 500 μg/ml Hoechst (Sigma-Aldrich) was used to visualize DNA.

Cells were imaged with an Opera Phenix high-content screening system (Perkin-Elmer) using its confocal spinning disk mode with either a $\times$20 water immersion objective lens (Perkin-Elmer, NA 1.0, WD 1.7 mm) or a $\times$63 water immersion objective lens (Perkin-Elmer, NA 1.15, WD 0.6 mm) and the system's two sCMOS cameras (4.4-megapixel 2,100 $\times$ 2,100, 16-bit resolution, 6.5-μm pixel size). Image analysis was carried out using Harmony high-content imaging and analysis software (Perkin-Elmer) on 16-bit images. All analysis was done using maximum-intensity projections except for nuclear and cytoplasmic actin quantification, which was done on single z-plane images through the center of cell nuclei.

Electron microscopy. Sf9 cells were infected in triplicate with WOBpos or AC102-K66A virus at an MOI of 10, and infected cells were fixed at 18 and 36 hpi for 45 min with 1.5% paraformaldehyde and 2.0% glutaraldehyde in 0.05 M sodium cacodylate buffer (pH 7.3). Cell pellets were embedded in 2% agarose, rinsed three times in 0.05 M sodium cacodylate buffer (pH 7.3), and postfixed in a solution of 1% osmium tetroxide, 1.6% potassium ferricyanide, and 0.1 M sodium cacodylate buffer (pH 7.2). Postfixed samples were then embedded in resin, sectioned, stained with 2% uranyl acetate in 70% methanol, rinsed in decreasing concentrations of methanol, and stained with Reynolds lead citrate. Samples were imaged with a FEI Tecnai 12 transmission electron microscope (Thermo Fisher Scientific) equipped with a 3,072 $\times$ 3,072 pixel Rio 9 CMOS camera (Gatan).

ACKNOWLEDGMENTS

We thank Loy Volkman for the rabbit anti-polyhedrin antibody, Linda Guarino for the rabbit anti-PP31 antibody, Michael Goldberg and Kris Gunsalus for the rabbit anti-cofilin GA15 antibody, and JaRue Manning for the mouse anti-VP39 P10C6 antibody. We also thank Kent McDonald and Reena Zalpuri from the Robert D. Ogg Electron Microscope Lab, Lori Kohlstaedt from the Vincent J. Coates Proteomics/Mass Spectrometry Laboratory, and Mary West from the QB3 High-Throughput Screening Facility for use of the facilities and technical support. We are grateful to Loy Volkman for advice, support, helpful suggestions, and comments on the manuscript.

This study was supported by a Hellman Graduate Award to S.E.H. and by NIH/NIGMS grant R01 GM059609 to M.D.W.

REFERENCES

1. Rohrmann GF. 2013. Baculovirus molecular biology: 3rd ed. National Center for Biotechnology Information, Bethesda, MD.
2. Kost TA, Kemp CW. 2016. Fundamentals of baculovirus expression and applications. Adv Exp Med Biol 896:187–197. https://doi.org/10.1007/978-3-319-27216-0_12.
3. Haglund CM, Welch MD. 2011. Pathogens and polymers: microbe-host

interactions illuminate the cytoskeleton. J Cell Biol 195:7–17. https://doi.org/10.1083/jcb.201103148.
4. Welch MD, Way M. 2013. Arp2/3-mediated actin-based motility: a tail of pathogen abuse. Cell Host Microbe 14:242–255. https://doi.org/10.1016/j.chom.2013.08.011.
5. Charlton CA, Volkman LE. 1991. Sequential rearrangement and nuclear polymerization of actin in baculovirus-infected *Spodoptera frugiperda* cells. J Virol 65:1219–1227.
6. Charlton CA, Volkman LE. 1993. Penetration of *Autographa californica* nuclear polyhedrosis virus nucleocapsids into IPLB Sf21 cells induces actin cable formation. Virology 197:245–254. https://doi.org/10.1006/viro.1993.1585.
7. Volkman LE, Goldsmith PA, Hess RT. 1987. Evidence for microfilament involvement in budded *Autographa californica* nuclear polyhedrosis virus production. Virology 156:32–39. https://doi.org/10.1016/0042-6822(87)90433-8.
8. Ohkawa T, Volkman LE. 1999. Nuclear F-actin is required for AcMNPV nucleocapsid morphogenesis. Virology 264:1–4. https://doi.org/10.1006/viro.1999.0008.
9. Goley ED, Ohkawa T, Mancuso J, Woodruff JB, D'Alessio JA, Cande WZ, Volkman LE, Welch MD. 2006. Dynamic nuclear actin assembly by Arp2/3 complex and a baculovirus WASP-like protein. Science 314:464–467. https://doi.org/10.1126/science.1133348.
10. Hess RT, Goldsmith PA, Volkman LE. 1989. Effect of cytochalasin D on cell morphology and AcMNPV replication in a *Spodoptera frugiperda* cell line. J Invertebr Pathol 53:169–182. https://doi.org/10.1016/0022-2011(89)90005-0.
11. Kasman LM, Volkman LE. 2000. Filamentous actin is required for lepidopteran nucleopolyhedrovirus progeny production. J Gen Virol 81:1881–1888. https://doi.org/10.1099/0022-1317-81-7-1881.
12. Ohkawa T, Volkman LE, Welch MD. 2010. Actin-based motility drives baculovirus transit to the nucleus and cell surface. J Cell Biol 190:187–195. https://doi.org/10.1083/jcb.201001162.
13. Ohkawa T, Rowe AR, Volkman LE. 2002. Identification of six *Autographa californica* multicapsid nucleopolyhedrovirus early genes that mediate nuclear localization of G-actin. J Virol 76:12281–12289. https://doi.org/10.1128/JVI.76.23.12281-12289.2002.
14. Gandhi KM, Ohkawa T, Welch MD, Volkman LE. 2012. Nuclear localization of actin requires AC102 in *Autographa californica* multiple nucleopolyhedrovirus-infected cells. J Gen Virol 93:1795–1803. https://doi.org/10.1099/vir.0.041848-0.
15. Ono C, Kamagata T, Taka H, Sahara K, Asano S-I, Bando H. 2012. Phenotypic grouping of 141 BmNPVs lacking viral gene sequences. Virus Res 165:197–206. https://doi.org/10.1016/j.virusres.2012.02.016.
16. Machesky LM, Insall RH, Volkman LE. 2001. WASP homology sequences in baculoviruses. Trends Cell Biol 11:286–287. https://doi.org/10.1016/S0962-8924(01)02009-8.
17. Braunagel SC, Guidry PA, Rosas-Acosta G, Engelking L, Summers MD. 2001. Identification of BV/ODV-C42, an *Autographa californica* nucleopolyhedrovirus orf101-encoded structural protein detected in infected-cell complexes with ODV-EC27 and p78/83. J Virol 75:12331–12338. https://doi.org/10.1128/JVI.75.24.12331-12338.2001.
18. Russell RL, Funk CJ, Rohrmann GF. 1997. Association of a baculovirus-encoded protein with the capsid basal region. Virology 227:142–152. https://doi.org/10.1006/viro.1996.8304.
19. Possee RD, Sun TP, Howard SC, Ayres MD, Hill-Perkins M, Gearing KL. 1991. Nucleotide sequence of the *Autographa californica* nuclear polyhedrosis 9.4-kbp EcoRI-I and -R (polyhedrin gene) region. Virology 185:229–241. https://doi.org/10.1016/0042-6822(91)90770-C.
20. Vanarsdall AL, Pearson MN, Rohrmann GF. 2007. Characterization of baculovirus constructs lacking either the Ac101, Ac142, or the Ac144 open reading frame. Virology 367:187–195. https://doi.org/10.1016/j.virol.2007.05.003.
21. Chen Y-R, Zhong S, Fei Z, Hashimoto Y, Xiang JZ, Zhang S, Blissard GW. 2013. The transcriptome of the baculovirus *Autographa californica* multiple nucleopolyhedrovirus in *Trichoplusia ni* cells. J Virol 87:6391–6405. https://doi.org/10.1128/JVI.00194-13.
22. Thiem SM, Miller LK. 1989. Identification, sequence, and transcriptional mapping of the major capsid protein gene of the baculovirus *Autographa californica* nuclear polyhedrosis virus. J Virol 63:2008–2018.
23. Lu A, Craig A, Casselman R, Carstens EB. 1996. Nucleotide sequence, insertional mutagenesis, and transcriptional mapping of a conserved region of the baculovirus *Autographa californica* nuclear polyhedrosis virus (map unit 64.8 to 66.9). Can J Microbiol 42:1267–1273. https://doi.org/10.1139/m96-165.
24. Guarino LA, Dong W, Xu B, Broussard DR, Davis RW, Jarvis DL. 1992. Baculovirus phosphoprotein pp31 is associated with virogenic stroma. J Virol 66:7113–7120.
25. Schmidt TGM, Batz L, Bonet L, Carl U, Holzapfel G, Kiem K, Matulewicz K, Niermeier D, Schuchardt I, Stanar K. 2013. Development of the Twin-Strep-tag and its application for purification of recombinant proteins from cell culture supernatants. Protein Expr Purif 92:54–61. https://doi.org/10.1016/j.pep.2013.08.021.
26. Braunagel SC, Russell WK, Rosas-Acosta G, Russell DH, Summers MD. 2003. Determination of the protein composition of the occlusion-derived virus of *Autographa californica* nucleopolyhedrovirus. Proc Natl Acad Sci U S A 100:9797–9802. https://doi.org/10.1073/pnas.1733972100.
27. Deng F, Wang R, Fang M, Jiang Y, Xu X, Wang H, Chen X, Arif BM, Guo L, Wang H, Hu Z. 2007. Proteomics analysis of *Helicoverpa armigera* single nucleocapsid nucleopolyhedrovirus identified two new occlusion-derived virus-associated proteins, HA44 and HA100. J Virol 81:9377–9385. https://doi.org/10.1128/JVI.00632-07.
28. Wang R, Deng F, Hou D, Zhao Y, Guo L, Wang H, Hu Z. 2010. Proteomics of the *Autographa californica* nucleopolyhedrovirus budded virions. J Virol 84:7233–7242. https://doi.org/10.1128/JVI.00040-10.
29. Oppenheimer DI, Volkman LE. 1995. Proteolysis of p6.9 induced by cytochalasin D in *Autographa californica* M nuclear polyhedrosis virus-infected cells. Virology 207:1–11. https://doi.org/10.1006/viro.1995.1046.
30. Volkman LE. 1988. *Autographa californica* MNPV nucleocapsid assembly: inhibition by cytochalasin D. Virology 163:547–553. https://doi.org/10.1016/0042-6822(88)90295-4.
31. Vanarsdall AL, Okano K, Rohrmann GF. 2006. Characterization of the role of very late expression factor 1 in baculovirus capsid structure and DNA processing. J Virol 80:1724–1733. https://doi.org/10.1128/JVI.80.4.1724-1733.2006.
32. Wu W, Lin T, Pan L, Yu M, Li Z, Pang Y, Yang K. 2006. *Autographa californica* multiple nucleopolyhedrovirus nucleocapsid assembly is interrupted upon deletion of the 38K gene. J Virol 80:11475–11485. https://doi.org/10.1128/JVI.01155-06.
33. Marek M, Romier C, Galibert L, Merten O-W, van Oers MM. 2013. Baculovirus VP1054 is an acquired cellular PURα, a nucleic acid-binding protein specific for GGN repeats. J Virol 87:8465–8480. https://doi.org/10.1128/JVI.00068-13.
34. Guan Z, Zhong L, Li C, Wu W, Yuan M, Yang K. 2016. The *Autographa californica* multiple nucleopolyhedrovirus *ac54* gene is crucial for localization of the major capsid protein VP39 at the site of nucleocapsid assembly. J Virol 90:4115–4126. https://doi.org/10.1128/JVI.02885-15.
35. Liu C, Li Z, Wu W, Li L, Yuan M, Pan L, Yang K, Pang Y. 2008. *Autographa californica* multiple nucleopolyhedrovirus *ac53* plays a role in nucleocapsid assembly. Virology 382:59–68. https://doi.org/10.1016/j.virol.2008.09.003.
36. Liang C, Li M, Dai X, Zhao S, Hou Y, Zhang Y, Lan D, Wang Y, Chen X. 2013. *Autographa californica* multiple nucleopolyhedrovirus PK-1 is essential for nucleocapsid assembly. Virology 443:349–357. https://doi.org/10.1016/j.virol.2013.05.025.
37. Katsuma S, Kokusho R. 2017. A conserved glycine residue is required for proper functioning of a baculovirus VP39 protein. J Virol 91:e02253-16. https://doi.org/10.1128/JVI.02253-16.
38. Li K, Wang Y, Bai H, Wang Q, Song J, Zhou Y, Wu C, Chen X. 2010. The putative pocket protein binding site of *Autographa californica* nucleopolyhedrovirus BV/ODV-C42 is required for virus-induced nuclear actin polymerization. J Virol 84:7857–7868. https://doi.org/10.1128/JVI.00174-10.
39. Wang Y, Wang Q, Liang C, Song J, Li N, Shi H, Chen X. 2008. *Autographa californica* multiple nucleopolyhedrovirus nucleocapsid protein BV/ODV-C42 mediates the nuclear entry of P78/83. J Virol 82:4554–4561. https://doi.org/10.1128/JVI.02510-07.
40. Tischer BK, Smith GA, Osterrieder N. 2010. En passant mutagenesis: a two step markerless red recombination system. Methods Mol Biol 634:421–430. https://doi.org/10.1007/978-1-60761-652-8_30.
41. Volkman LE, Goldsmith PA. 1982. Generalized immunoassay for *Autographa californica* nuclear polyhedrosis virus infectivity in vitro. Appl Environ Microbiol 44:227–233.
42. Edelstein AD, Tsuchida MA, Amodaj N, Pinkard H, Vale RD, Stuurman N. 2014. Advanced methods of microscope control using μManager software. J Biol Methods 1:10. https://doi.org/10.14440/jbm.2014.36.

43. Schindelin J, Arganda-Carreras I, Frise E, Kaynig V, Longair M, Pietzsch T, Preibisch S, Rueden C, Saalfeld S, Schmid B, Tinevez J-Y, White DJ, Hartenstein V, Eliceiri K, Tomancak P, Cardona A. 2012. Fiji: an open-source platform for biological-image analysis. Nat Methods 9:676–682. https://doi.org/10.1038/nmeth.2019.
44. Rosenfeld J, Capdevielle J, Guillemot JC, Ferrara P. 1992. In-gel digestion of proteins for internal sequence analysis after one- or two-dimensional gel electrophoresis. Anal Biochem 203:173–179. https://doi.org/10.1016/0003-2697(92)90061-B.
45. Washburn MP, Wolters D, Yates JR. 2001. Large-scale analysis of the yeast proteome by multidimensional protein identification technology. Nat Biotechnol 19:242–247. https://doi.org/10.1038/85686.
46. Xu T, Park SK, Venable JD, Wohlschlegel JA, Diedrich JK, Cociorva D, Lu B, Liao L, Hewel J, Han X, Wong CCL, Fonslow B, Delahunty C, Gao Y, Shah H, Yates JR. 2015. ProLuCID: an improved SEQUEST-like algorithm with enhanced sensitivity and specificity. J Proteomics 129:16–24. https://doi.org/10.1016/j.jprot.2015.07.001.
47. Tabb DL, McDonald WH, Yates JR. 2002. DTASelect and Contrast: tools for assembling and comparing protein identifications from shotgun proteomics. J Proteome Res 1:21–26. https://doi.org/10.1021/pr015504q.
48. Cociorva D, L Tabb D, Yates JR. 2007. Validation of tandem mass spectrometry database search results using DTASelect. Curr Protoc Bioinformatics Chapter 13: Unit 13.4.
49. Park SK, Venable JD, Xu T, Yates JR. 2008. A quantitative analysis software tool for mass spectrometry-based proteomics. Nat Methods 5:319–322. https://doi.org/10.1038/nmeth.1195.
50. McDonald WH, Tabb DL, Sadygov RG, MacCoss MJ, Venable J, Graumann J, Johnson JR, Cociorva D, Yates JR. 2004. MS1, MS2, and SQT-three unified, compact, and easily parsed file formats for the storage of shotgun proteomic spectra and identifications. Rapid Commun Mass Spectrom 18:2162–2168. https://doi.org/10.1002/rcm.1603.
51. Peng J, Elias JE, Thoreen CC, Licklider LJ, Gygi SP. 2003. Evaluation of multidimensional chromatography coupled with tandem mass spectrometry (LC/LC-MS/MS) for large-scale protein analysis: the yeast proteome. J Proteome Res 2:43–50. https://doi.org/10.1021/pr025556v.
52. Goldfarb D, Hast BE, Wang W, Major MB. 2014. Spotlite: web application and augmented algorithms for predicting co-complexed proteins from affinity purification–mass spectrometry data. J Proteome Res 13:5944–5955. https://doi.org/10.1021/pr5008416.
53. Guruharsha KG, Rual J-F, Zhai B, Mintseris J, Vaidya P, Vaidya N, Beekman C, Wong C, Rhee DY, Cenaj O, McKillip E, Shah S, Stapleton M, Wan KH, Yu C, Parsa B, Carlson JW, Chen X, Kapadia B, VijayRaghavan K, Gygi SP, Celniker SE, Obar RA, Artavanis-Tsakonas S. 2011. A protein complex network of *Drosophila melanogaster*. Cell 147:690–703. https://doi.org/10.1016/j.cell.2011.08.047.
54. Whitt MA, Manning JS. 1988. A phosphorylated 34-kDa protein and a subpopulation of polyhedrin are thiol linked to the carbohydrate layer surrounding a baculovirus occlusion body. Virology 163:33–42. https://doi.org/10.1016/0042-6822(88)90231-0.
55. Volkman LE. 1983. Occluded and budded *Autographa californica* nuclear polyhedrosis virus: immunological relatedness of structural proteins. J Virol 46:221–229.
56. Katoh K, Rozewicki J, Yamada KD. 2017. MAFFT online service: multiple sequence alignment, interactive sequence choice, and visualization. Brief Bioinform 30:3059. https://doi.org/10.1093/bib/bbx108.